12^{th} International Conference on Fracture Mechanics of Concrete and Concrete Structures
FraMCoS-12
B.L.A. Pichler, Ch. Hellmich, P. Preinstorfer (Eds)

https://doi.org/10.21012/FC12.1158
MS01-2:1

FRACTURE MECHANICS-BASED MODEL FOR THE FLEXURAL BEHAVIOR OF STEEL FIBER-REINFORCED CONCRETE WITH LONGITUDINAL REINFORCEMENT

ÁNGEL DE LA ROSA*, GONZALO RUIZ†, AND JACINTO R. CARMONA‡

* DIMME, Grupo de Durabilidad e Integridad Mecánica de Materiales Estructurales,
Universidad Rey Juan Carlos
C. Tulipán s/n, 28933 Móstoles, Madrid, Spain
e-mail: angel.delarosa@urjc.es, www.urjc.es

†ETSI Caminos, C. y P., Universidad de Castilla-La Mancha
Av. Camilo José Cela 2, 13071 Ciudad Real, Spain
e-mail: gonzalo.ruiz@uclm.es, www.uclm.es

†ETS de Arquitectura, Universidad Politécnica de Madrid
Campus de Moncloa, 28049 Madrid, Spain
e-mail: jacinto.ruiz@upm.es, www.upm.es

Key words: Analytical flexural model for steel-fiber reinforced concrete, Longitudinal reinforcement, Fracture mechanics, Crack propagation, Size effect.

Abstract. This study introduces an analytical model to evaluate the flexural strength of concrete sections with longitudinal reinforcement and steel fibers based on Fracture Mechanics principles. It combines the compressive behavior model from Eurocode 2 with the tensile softening model from Model Code 2010 to accurately simulate the compressive and tensile responses of concrete. The model adopts a parabolic-linear stress-strain relationship for compression and a linear softening law for tension under the flat crack hypothesis. By ensuring compatibility between crack openings and reinforcement elongation, it facilitates precise analyses of stress distribution and fracture depth. The results highlight significant size effects governed by the brittleness number, which accounts for element size, tensile softening, and residual flexural strength. This model provides a practical and reliable tool for predicting the flexural behavior of concrete configurations with low longitudinal reinforcement ratios.

1 INTRODUCTION

The post-cracking behavior of steel fiber reinforced concrete elements results from the interaction between the stress-crack opening relationship in the tensile zone and the stress-strain response in the compression zone [1]. The fibers' bridging action plays a key role in ductile behavior by stitching crack faces together after cracking [2]. The size effect in concrete, particularly the fracture process zone (FPZ) [3], is influenced by fiber inclusion, which extends the FPZ [4,5]. Two models, the Fictitious Crack Model and the Smeared Crack Band Model, effectively describe the post-cracking softening behavior and residual strength [4,6]. The size of the Fracture Process Zone (FPZ), which plays a crucial role in load capacity calculations, is influenced by the material's heterogeneity and energy dissipation mechanisms [7,8]. Additionally, the presence of steel fibers alters the devel-

opment of the FPZ by modifying the material's properties [9, 10].

This study introduces an analytical model for evaluating the flexural behavior of reinforced concrete with longitudinal reinforcement and steel fibers. The model integrates Eurocode 2 for compressive response and Model Code 2010 for tensile softening [11]. It uses a linear stress-crack opening softening law, incorporating compatibility equations to link crack opening with reinforcement elongation [12]. The model accurately represents bending performance, crack propagation, and stress distribution, providing a reliable tool for structural design and failure analysis.

2 INITIAL SPECIFICATIONS

This framework outlines a sectional analysis model for evaluating the impact of a low longitudinal reinforcement ratio and steel fibers on concrete's flexural behavior:

- Hybrid reinforcement effectiveness: Combines longitudinal bars and steel fibers for enhanced crack control under flexural loads.
- Parabolic-linear compression model: Captures pre- and post-peak compressive behavior, as defined in Eurocode 2 [13], accurately representing the ductility of the compressive zone.
- Flexural strength and ductility: Influenced by material ductility, reinforcement ratio, ρ, adhesion η, and brittleness number, $\beta_{H,f}$, with specific practical ranges for steel-fiber concrete.
- Minimum reinforcement requirements: Eurocode 2 [13] mandates minimum longitudinal reinforcement for crack control, even with steel fibers.
- Size effects and Fracture Mechanics: Crack propagation is affected by the size, the cover thickness, the reinforcement adhesion, and the fracture process zone.
- Model scope: Applies to crack widths $w \leq w_u$ = 2.5 mm (w_u is the the ultimate crack value), covering flexural strength classes 1–8 a/b, and uses the softening law from Eurocode 2 [13].
- Critical section depth: Defines critical cover thickness to prevent premature reinforcement fracture and ensure load-bearing capacity.

2.1 Criteria for failure and plastic deformation rotation

In a rectangular steel-fiber reinforced concrete section, bending deformation occurs at the section's center, where the bending moment is highest ($M = \frac{PL}{4}$). Failure is marked by the formation of a dominant flexural crack, occurring when the crack opening reaches a critical value, w_c, or the strain in the upper compressed fiber exceeds its maximum limit, ϵ_{cu}.

The horizontal displacement in the compression zone, Δ_c, can be determined from the strain distribution along the longitudinal direction [2] and is related with the rotation angle of the section's axis, given by Eq. (1):

$$d\theta \approx \frac{\Delta_c}{2c} \tag{1}$$

The crack opening, w, is expressed by Eq. (2) and is related to the rotation by Eq. (3):

$$dw = 2\left[d\theta\,(h-c)\right] \tag{2}$$

$$w = 2\,\theta\,(h-c) \tag{3}$$

being h the eight of the section of the structural element and c the depth of the neutral fiber from the upper face of the structural element. The strain in the upper compressed fiber and the crack mouth opening at the lower fiber are related by Eq. (4):

$$\epsilon_c = \frac{2\Delta_c}{L} = \frac{2wc}{L(h-c)} \tag{4}$$

being L the length of the structural element. For longitudinal reinforcement, failure occurs when either the maximum strain in the steel,

ε_{su}, or in the concrete, ε_{cu}, is reached. The strain in the steel bar, ε_s, is given by Eq. (5):

$$\varepsilon_s = \frac{2\Delta l_s}{l_b} \tag{5}$$

where Δl_s represents the elongation of the steel bar and l_b its length. For the failure mode, the relationship between the critical crack opening w_c and section rotation is given by Eq. (6):

$$\tan\theta = \frac{w_c}{2(z-d)} \approx \theta = \frac{w_c}{2(z-d)} \tag{6}$$

In dimensionless terms (Eq. (7)):

$$\theta = \frac{w_c^*}{2(\xi-\zeta)} \tag{7}$$

where z is the crack depth at which stress transmission occurs, ξ is the dimensionless crack depth, d is the cover rebar, and $\zeta = d/h$ represents the dimensionless cover rebar.

Figure 1 depicts the failure behavior of a concrete beam section with longitudinal reinforcement and steel fibers under a three-point bending load, assessing the rotational capacity and correlating each critical crack opening, w_c, with the beam's rotation, as defined in Eq. (6).

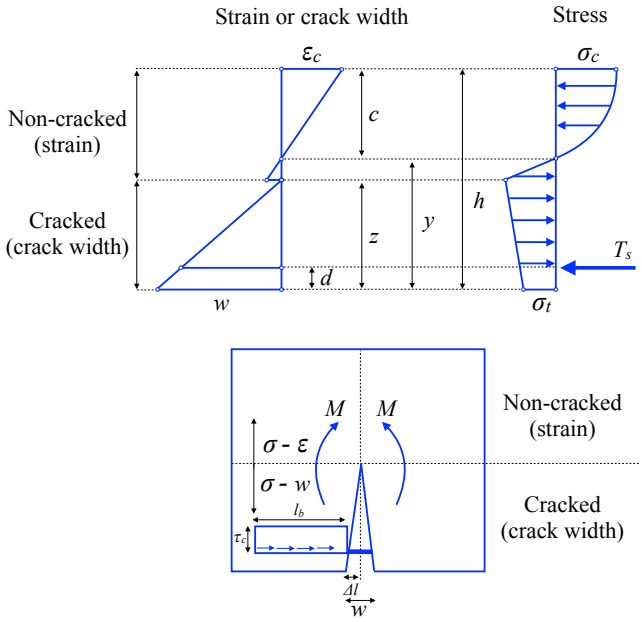

Figure 1: Mode of failure in a concrete beam with longitudinal reinforcement and steel fibers subjected to a three-point bending test.

2.2 Stress allocation within the ligament of the structural component

The post-cracking behavior of the structural element is determined by the material's stress-strain response under bending and the stress-crack opening relationship after crack initiation [1]. Figure 2 shows the stress-strain distribution in the ligament under three-point bending, with stress-strain in compression and stress-crack opening in tension. The compressive stress distribution in the uncracked region, before and after peak compression, is defined by the dimensionless stress-strain model $\sigma - \epsilon$, proposed by Ruiz *et al.* [14], and adopted in Eurocode 2 [13].

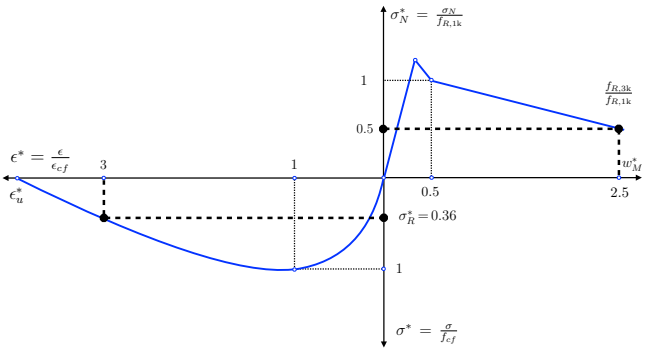

Figure 2: Non-dimensional model for the bending response of steel fiber-reinforced concrete (modified from Ruiz *et al.* [16]).

3 HYPOTHESES FOR SIMULATING CRACK GROWTH BEHAVIOR

Two hypotheses are required: one for the uncracked zone and another for the cracked zone, depending on whether the material's tensile strength has been reached.

3.1 Uncracked zone

In the uncracked region, tension follows a linear elastic stress-strain relationship, with Navier's plane section hypothesis for compatibility. For compression, the model uses the stress-strain relation for steel fiber-reinforced concrete from Annex L of Eurocode 2 [13]. Alternatively, a parabolic-rectangular stress distribution is proposed, reaching maximum compressive strength at the centroid of the stress block. Compressive failure is prevented due to

the fibers' energy absorption, rotation, and ductility in the compression zone, even as the crack approaches the element's edge.

3.2 Cracked zone

3.2.1 Role of steel fiber reinforcement in tension

In the cohesive model for post-cracking behavior of steel-fiber reinforced concrete, a linear stress-crack mouth opening relationship, $\sigma - w$, is proposed for uniaxial tension (Fig. 3) [11]. The post-cracking flexural residual strengths f_{Fts} and f_{Ftu} (f_{Fts} is the post-cracking flexural residual strength for the crack opening limit state in service, and f_{Ftu} is the post-cracking flexural residual strength for ultimate crack opening limit state):

$$f_{Fts} = 0.45\, f_{R1} \tag{8}$$

$$\begin{aligned} f_{Ftu} &= f_{Fts} - \frac{w_u}{CMOD_3}\left(f_{Fts} - 0.5\, f_{R3} + 0.2\, f_{R1}\right) \\ &= 0.5\, f_{R3} - 0.2\, f_{R1} \end{aligned} \tag{9}$$

where f_{R1} is the flexural residual strength for a crack mouth opening value equal to 0.5 mm and f_{R3} is the flexural residual strength for a crack mouth opening value equal to 2.5 mm. The crack opening, w, is given by Eq. (21):

$$w = \frac{f_{Fts} - \sigma}{f_{Fts} - f_{Ftu}}\, w_u \tag{10}$$

The fracture energy, $G_{F,f}$, is calculated by Eq. (11):

$$G_{F,f} = \frac{f_{Fts} + f_{Ftu}}{2}\, w_u; \quad w_u = \frac{2\, G_{F,f}}{f_{Fts} + f_{Ftu}} \tag{11}$$

In the uncracked zone, the plane sections hypothesis is applied for compatibility. Crack propagation begins just before maximum stress and continues with softening. Fiber reinforcement affects the softening response, and the crack profile remains planar after the proportional limit, leading to a linear stress profile across the cohesive bond in the element.

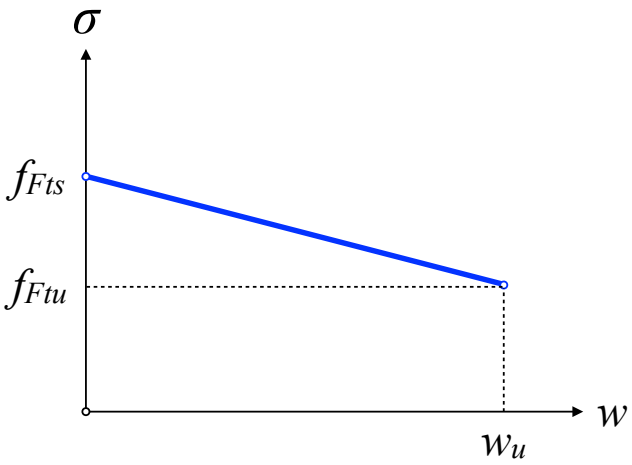

Figure 3: A simplified representation of the post-cracking softening behavior for steel-fiber reinforced concrete is presented in [11].

3.2.2 Role of longitudinal steel reinforcement in tension

The inclusion of longitudinal steel reinforcement in the concrete section introduces an additional tensile force, T_s, given by Eq. (12):

$$T_s = A_s \sigma_s \tag{12}$$

where A_s is the area of the steel reinforcement, σ_s the stress in the steel, and ρ the reinforcement ratio ($\rho = \frac{A_s}{bh}$, b is the width of the section of the structural element). This stress is represented in dimensionless form as $\sigma_s^* = \frac{\sigma_s}{f_{FTS}}$, simplifying calculations for crack propagation and section behavior.

The force equilibrium in the section is adjusted to include T_s, affecting the depth of the compression zone and the moment capacity of the section, as expressed by Eq. (13):

$$\frac{T_s}{bh f_{FTS}} = \rho \sigma_s^* \tag{13}$$

The depth of the compression resultant is determined from force equilibrium, and the moment at a given crack depth is expressed as the dimensionless value $M^* = \frac{M}{bh^2 f_{FTS}}$.

The model links the steel strain in the crack zone to the crack width w. Assuming bar elongation corresponds to half the crack opening, the elongation, Δl, is calculated using the shear

stress between steel and concrete and the bar perimeter, τ_c, (see Fig. 1). The dimensionless steel stress is derived by substituting into the equilibrium equations, introducing η, a bond-related parameter that adjusts stress transfer from steel to concrete, defined as Eq. (14) [12]:

$$\eta = \sqrt{\frac{E_s}{E_c}\,\frac{\tau_c}{f_{FTS}}\,\frac{p_e\,\ell_{ch}}{A_s}} \tag{14}$$

where E_s and E_c are the moduli of elasticity of steel and concrete, respectively, τ_c is the shear stress at the interface between steel and concrete, and p_e is the perimeter of the longitudinal steel reinforcement. An elastic-perfectly plastic behavior is assumed for the steel rebar.

3.2.3 Role of steel fiber reinforcement in compression

To analyze the complete flexural response of steel fiber-reinforced concrete structural elements, it is essential to incorporate a model that accurately represents the behavior of the compressed zone within the section. We apply the model proposed by Ruiz *et al.* [14,15], included in Annex L of Eurocode 2 [13], as shown in Fig. 4.

According to Eurocode 2 [13], other idealized stress-strain relationships may be applied if they adequately represent the behavior of the concrete. The parabolic-linear model for steel fiber-reinforced concrete characterizes the compressive behavior before and after peak load. Initially, a parabolic segment describes the material's response up to maximum compressive strength, transitioning into a linear or rectangular softening phase. This approach, known as the parabolic-rectangle model, is ideal for sectional analysis, as it captures the ductile behavior in the compressive zone, improving load-bearing predictions and crack control. The model assumes that the steel reinforcement remains within its elastic range, avoiding plastic deformation effects.

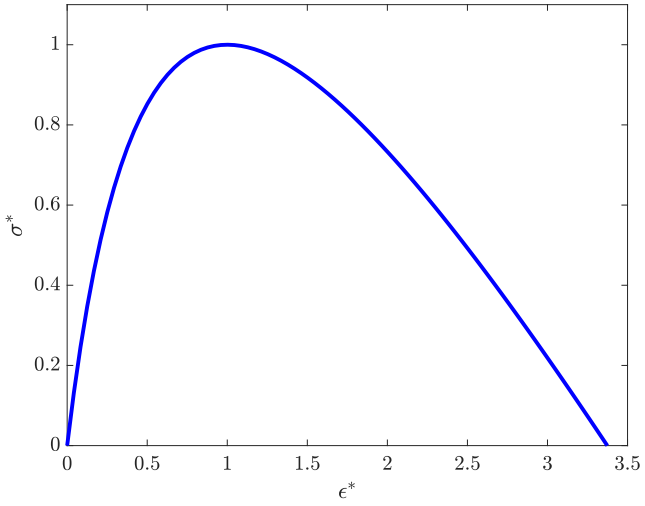

Figure 4: A dimensionless model describing the compressive behavior of SFRC is discussed in [13–15].

3.2.4 Crack propagation

A rectangular concrete section with height h and width b, reinforced with longitudinal steel bars and steel fibers, is considered under crack progression conditions. The damage process zone develops at the crack tip, reflecting the quasi-brittle behavior of concrete. Fig. 5 shows the section subjected to a three-point bending test.

The parameters are defined as follows:

- h: height of the section.
- b: width of the section.
- z: crack depth at which stress transmission occurs.
- z_0: tension-free crack depth.
- y: neutral axis depth (from bottom face).
- c': depth from maximum compressive stress to the neutral axis.
- d: concrete cover over steel reinforcement ($d = 0.1\,h$).

The geometric dimensions are normalized by dividing by h (section height):

- $\xi = \frac{z}{h}$: dimensionless crack depth.

- $\xi_0 = \frac{z_0}{h}$: dimensionless tensile-free crack depth.
- $\gamma = \frac{y}{h}$: dimensionless neutral axis depth (from bottom fiber).
- $\delta = \frac{c}{h}$: dimensionless neutral axis depth (from top fiber).
- $\rho = \frac{c'}{h}$: dimensionless depth from max compressive stress to neutral axis.
- $\mu = \frac{d}{h}$: dimensionless depth from top fiber to max compressive stress.
- $\zeta = \frac{d}{h}$: dimensionless cover.

The crack opening is also dimensionless, $w^* = \frac{w}{w_u}$. The tensile and compressive stresses at the bottom and top fibers are denoted σ_t and σ_c, respectively, and are normalized as $\sigma_t^* = \frac{\sigma_t}{f_{Fts}}$ and $\sigma_c^* = \frac{\sigma_c}{f_{Fts}}$.

The crack propagation is divided into two situations:

- *Situation 1*: $w < w_u$ (Fig. 5(a), 5(b)).
- *Situation 2*: $w > w_u$ (tension-free crack, Fig. 5(c)).

In *Situation 1*, the crack depth at the critical opening z_0 increases monotonically. Two cases are considered:

- *Case a*: $\epsilon_c < \epsilon_{c1} = 0.0025$, and crack opening $w < w_u$.
- *Case b*: $\epsilon_c > \epsilon_{c1}$ but $\epsilon_c < \epsilon_{cu} = 0.006$, and crack opening $w \leq w_u$.

The maximum bending moment is reached when strain is below or above the concrete's compressive strength, depending on material properties and crack opening behavior. The ductility provided by fibers ensures that the maximum moment occurs after reaching the post-peak region if crack opening is large.

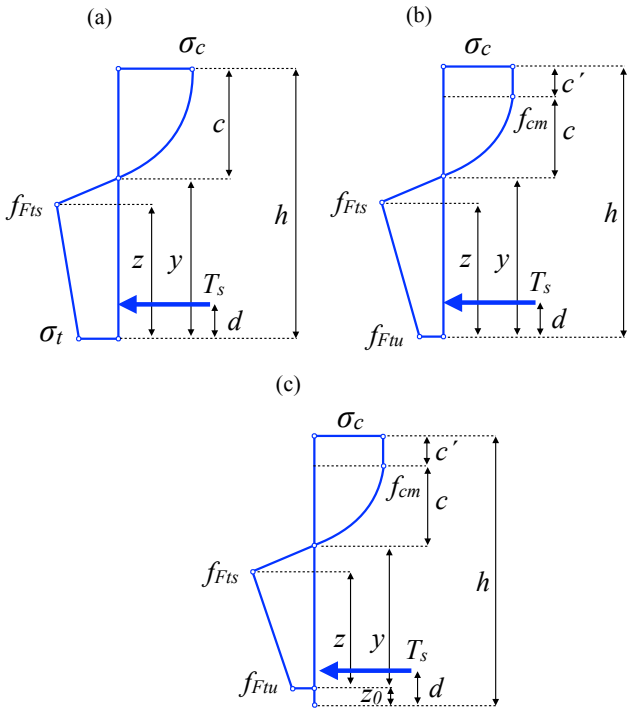

Figure 5: Ssimplified model for the softening behavior after cracking in a steel-fiber reinforced concrete section [11].

3.3 Situation 1 and case b: $\epsilon_{c1} \leq \epsilon_c \leq \epsilon_{cu}$, $w \leq w_u$

The objective of this research is to develop a model for cases in which the compression zone reaches the ultimate limit state. The ultimate limit state is defined by the maximum compressive strain in the upper fiber, $\epsilon_c = 0.006$, and a maximum crack opening in the lower fiber, $w = 2.5$ mm. Additionally, the yield strain $\epsilon_y = 0.002$ and ultimate fracture strain $\epsilon_s = 0.01$ for the longitudinal steel reinforcement are specified. A compatibility equation is introduced to relate crack opening to the elongation of the reinforcement bar.

The model considers a linear-rectangular distribution of compressive stresses within the compression zone, reaching the concrete's compressive strength, f_{cm}. The dimensionless compressive strength f_{cm}^* is defined as f_{cm}/f_{Fts}, with the resultant compressive force at the centroid of this distribution. The equilibrium equation for horizontal forces is expressed by Eq. (15):

$$\sum \boldsymbol{F_h} = 0 : \quad f^*_{cm}\, f_{Fts}\, h\, \delta\, b - \frac{f^*_{cm}\, f_{Fts}}{2}\,(h - h\,\xi - h\,\delta)\, b - \frac{1}{2}\,(\sigma^*_t\, f_{Fts} + f_{Fts})\, h\,\xi\, b - \sigma_s\, A_s = 0 \tag{15}$$

In a dimensionless way, Eq. (15) is Eq. (16):

$$f^*_{cm} = \gamma\, - 1 + \frac{\gamma + \sigma^*_t\,\xi + 2\sigma^*_s\,\rho}{f^*_{cm}} \tag{16}$$

The bending moment is determined from moment equilibrium by Eq. (17):

$$\sum \boldsymbol{M} = 0 : \quad f_{cm}\, h\, \delta\, b - \left(h - h\,\xi - \frac{h\,\delta}{2}\right) + \frac{f_{cm}}{3}\,(h - h\,\xi - h\,\delta)^2\, b + \frac{f_{Fts}}{3}\,(h\,\xi - h\,\gamma)^2\, b + \left(\frac{f_{Fts} + \sigma_t}{2}\right) h\,\gamma \left[h\,\xi - h\,\gamma + \left(\frac{h\,\gamma(f_{Fts} + 2\sigma_t)}{3(f_{Fts} + \sigma_b)}\right)\right] b + \sigma_s\, A_s(h\,\xi - d) \tag{17}$$

And expressed in a dimensionless format (Eq. (18)):

$$M^* = \quad f^*_{cm}\,\delta\left(1 - \xi - \frac{\delta}{2}\right) + \frac{f^*_{cm}}{3}(1 - \xi - \delta)^2\, b + \frac{1}{3}(\gamma - \xi)^2 + \left(\frac{1 + \sigma_t}{2}\right)\xi\left[\gamma - \xi\left(\frac{2 + \sigma^*_t}{3(1 + \sigma^*_b)}\right)\right] + \sigma_s\,\rho(\xi - d) \tag{18}$$

The first compatibility equation follows Navier's hypothesis (Eq. (20)):

$$\frac{f_{cm}}{h - h\,\xi - h\,\delta} = \frac{f_{Fts}}{h\,\xi - h\,\gamma} \tag{19}$$

In a dimensionless way, Eq. (19) is Eq. (20):

$$\gamma = \frac{1 - h\,\delta + f^*_{cm}\,\xi}{f^*_{cm} + 1} \tag{20}$$

The second compatibility equation is related to the crack width w (Eq. (21)).

$$w(M, z) = w(\sigma_t) = \frac{24M}{b\,h^2\,E_c}\, z f(\xi) = \frac{f_{Fts}\, -\, \sigma}{f_{Fts}\, -\, f_{Ftu}}\, w_u \tag{21}$$

The dimensionless crack width on the lower face of the section, w^*, is expressed by Eq. (22):

$$w^* = 12\, M^*\, \beta_{H,f}\, \xi\, f(\xi)\, \left(\frac{1}{1 - \alpha}\right) \tag{22}$$

The dimensionless stress on the lower face of the section, σ^*_t, is given by Eq. (23).

$$\sigma^*_t = 1 - 12\, M^*\, \beta_{H,f}\, \xi\, f(\xi) \tag{23}$$

The dimensionless stress in the steel bars, σ^*_s, is described by Eq. (24).

$$\sigma^{*\,2}_s = 24\, M^*\, \eta^2\, \beta_{H,f}\, \xi\, f(\xi)\, \left(1 - \frac{\mu}{\xi}\right) \tag{24}$$

The brittleness number for steel-fiber reinforced concrete, $\beta_{H,f}$, is introduced by Eq. (25):

$$\beta_{H,f} = \frac{h}{\ell_{ch,f}} = \frac{2h(f_{Fts} - f_{Ftu})}{E_c w_u} \tag{25}$$

As a summary, the crack depth ξ is governed by Eq. (20), which defines the specimen depth, while the dimensionless crack opening w^* is given by Eq. (22). Additionally, the dimensionless stress in the steel bars σ_s is obtained from Eq. (24).

To analyze the stress distribution, crack opening, and bending moment at a specific crack depth ξ, the system of six equations must be solved: Eqs. (16), (18), (20), (22), (23), and (24). The variables in this system include σ^*_c, σ^*_t (equivalent to f_{Ftu}), M^*, γ, σ^*_t, and σ^*_s, with $\beta_{H,f}$ being the sole input parameter. The crack

depth, ξ, acts as a control variable during the cracking process, providing a unique equilibrium solution for each depth. The crack opening behavior is influenced by both brittleness and the α ratio, with $\beta_{H,f}$ being the only input parameter.

4 RESULTS AND DISCUSSION

This study enhances the accuracy of structural design for reinforced concrete sections by providing a model that incorporates longitudinal reinforcement and steel fiber content. It enables more precise predictions of flexural capacity and crack propagation, leading to safer and more efficient structural designs.

4.1 Response M^*–w^* of the model

This section examines the effect of the brittleness number, $\beta_{H,f}$, on the behavior of concrete sections reinforced with both longitudinal steel bars and steel fibers. Figure 6 shows the M^*–w^* curves during crack propagation for α (= $\frac{f_{Ftu}}{f_{Fts}}$) values of 0.7, 0.8 and 0.9, and $\beta_{H,f}$ values of 0.005, 0.002, and 0.0007, respectively, which are typical for fiber-reinforced concrete. The curves correspond to different longitudinal reinforcement values, represented by η and ρ. The results reveal that for the three values of α analyzed, the maximum M^* increases as the values of parameters η and ρ grow. Additionally, as $\beta_{H,f}$ decreases, the maximum M^* increases, especially for sections with higher values of longitudinal reinforcement η and ρ. The analysis, using moment versus crack opening curves instead of moment versus curvature, offers a more accurate depiction of the flexural behavior of fiber-reinforced concrete.

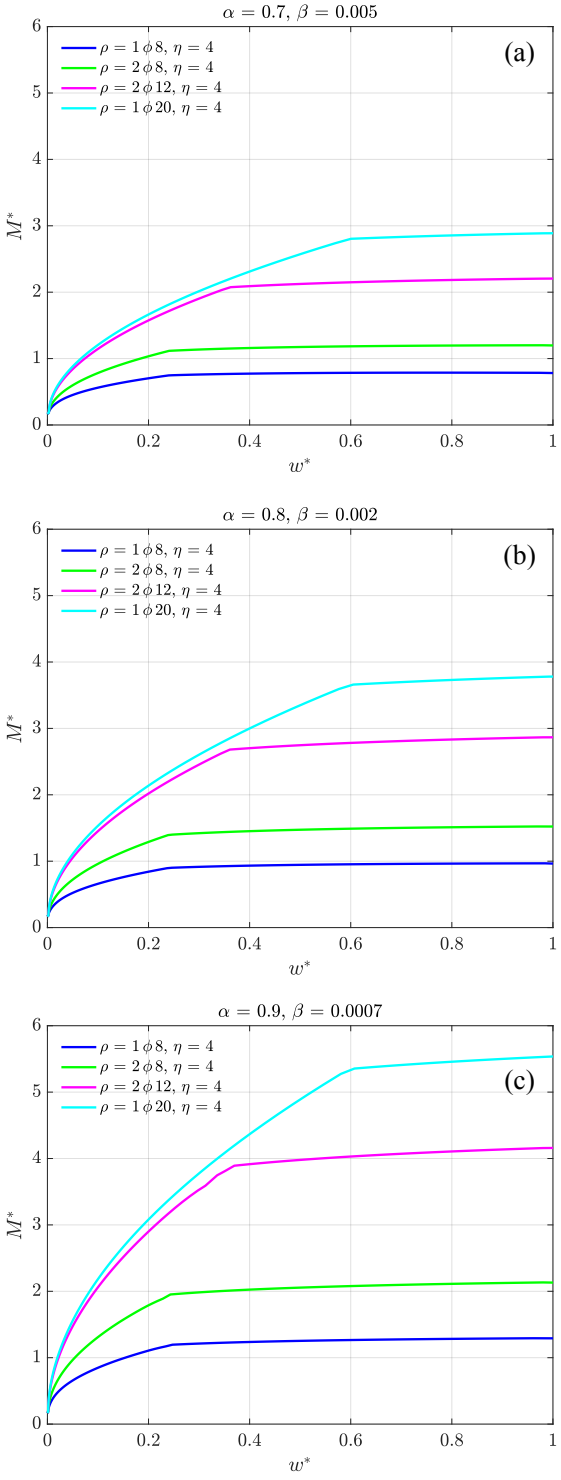

Figure 6: Relationship between the non-dimensional bending moment, M^*, and the non-dimensional crack mouth opening, w^*, for various values of η and ρ: (a) α = 0.7, (b) α = 0.8, (c) α = 0.9.

4.2 Size effect on flexural strength

As shown in Fig. 6, the maximum load value is determined as the absolute peak within

the dimensionless crack opening range [0, 1]. This maximum load is related to the flexural strength, f_R, as defined by Eq. (26):

$$f_R = \frac{6M_m}{bh^2} = \frac{6M_p^* bh^2 f_{Fts}}{bh^2} = 6M_m^* f_{Fts} \quad (26)$$

where M_m represents the maximum moment at section cracking, M_p^* is the dimensionless plastic moment, and M_m^* is the dimensionless maximum moment (both divided by f_{Fts}).

Figure 7 illustrates the relationship between the brittleness number, $\beta_{H,f}$, plotted on the x-axis, and the dimensionless flexural strength, f_R^*, the dimensionless bending moment, M^*, and the dimensionless crack depth corresponding to flexural strength, ξ_m, as functions of α. The results also account for the level of longitudinal reinforcement, represented by η and ρ.

Figure 7 demonstrates trends consistent with Fracture Mechanics models in steel-fiber reinforced concrete. Typically, $\beta_{H,f}$ for mass concrete ranges from 0.1 to 10, while for steel-fiber reinforced concrete, it is between 0.0001 and 0.1 [4]. Figure 7 shows the dependence of dimensionless parameters — f_R^*, M^*, and ξ_m — on $\beta_{H,f}$.

As $\beta_{H,f}$ approaches 0.0001, f_R^* converges in the range 2.5–3, indicating a plastic limit solution for cohesive cracks, as shown in Fig. 7 (a). Sections with longitudinal reinforcement and steel fibers under these conditions align with the linear portion of the cohesive crack plastic limit [4].

For typical $\beta_{H,f}$ values in steel-fiber reinforced concrete ([0.0001–0.01]) [4], the crack depth reaches significant levels, indicating that the fracture process zone covers a large portion of the section edge under maximum load.

Finally, the ratio $\frac{f_{Ftu}}{f_{Fts}} \leq 1$ aligns with the flexural strength classifications *a-c* in Model Code 2010 [11] and classes a–b in Annex L of Eurocode 2 [13]. Therefore, only classes 1–8 / a–b are suitable, as they satisfy the softening behavior requirements [13], confirming the applicability of this analytical model for structural design purposes.

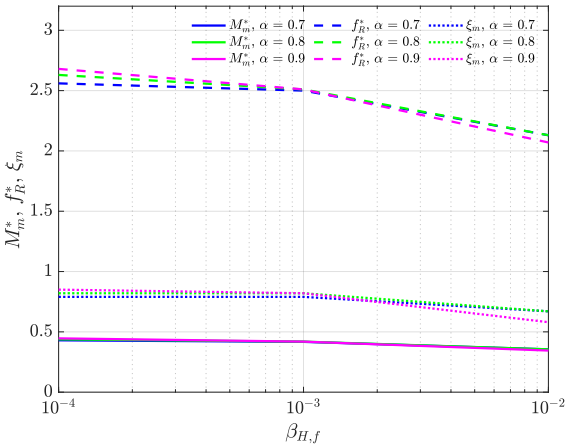

Figure 7: Correlation between the brittleness number, $\beta_{H,f}$, and the non-dimensional flexural strength, f_R^*, the non-dimensional bending moment, M^*, and the non-dimensional crack depth corresponding to the non-dimensional flexural strength, ξ_m.

5 CONCLUSIONS

This study introduces a novel analytical model for evaluating the flexural behavior of reinforced concrete with longitudinal reinforcement and steel fibers based on Fracture Mechanics. The model integrates Eurocode 2 for compression behavior and Model Code 2010 for post-cracking softening, providing accurate representations of bending, crack propagation, and concrete-steel bond interaction. A key feature is the compatibility equation linking crack opening with reinforcement elongation, ensuring realistic moment-crack opening correlations. The model accurately calculates the fracture zone depth, stress distribution, and accounts for the effects of the brittleness number, making it adaptable to various reinforced concrete scenarios. Dimensionless relationships for flexural strength, f_R^*, ultimate bending moment, M^*, and crack depth, ξ_m, provide practical insights for structural design. The model can also be adapted to account for different reinforcement ratios, bond strengths, and their influence on crack openings and failure modes. Future research should focus on experimental validation, large-scale effects, and integration into structural design software, further enhancing its practical application. This model advances predictive capabilities for reinforced concrete

bending, offering valuable insights for research and design.

REFERENCES

[1] Oh, B.H., Park, D.G., Kim, J.C., and Choi, Y.C. 2005. Experimental and theoretical investigation on the postcracking inelastic behavior of synthetic fiber reinforced concrete beams. *Cement and Concrete Research* **35**(2):384–392.

[2] Lee, S.C., Cho, J.Y., and Vecchio, F.J. 2013. Simplified diverse embedment model for steel fiber-reinforced concrete elements in tension. *Materials Journal* **110**(4):403–412.

[3] Bažant, Z.P. 1984. Size effect in blunt fracture: Concrete, rock, and mortar. *Journal of Engineering Mechanics* **110**:518–535.

[4] Carmona, J.R., Cortés-Buitrago, R., Rey-Rey, J., and Ruiz, G. 2022. Planar crack approach to evaluate the flexural strength of fiber-reinforced concrete sections. *Materials* **15**(17):5821.

[5] Li, V.C., and Liang, E. 1986. Fracture processes in concrete and fiber-reinforced cementitious composites. *ASCE Journal of Engineering Mechanics* **122**(6):566–586.

[6] Hillerborg, A., Modéer, M., and Petersson, P.E. 1976. Analysis of crack formation and crack growth in concrete by means of fracture mechanics and finite elements. *Cement and Concrete Research* **6**:773–782.

[7] Shah, S.P., Swartz, S.E., and Ouyang, C. 1995. *Fracture Mechanics of Concrete: Applications of Fracture Mechanics to Concrete, Rock and Other Quasi-Brittle Materials*. Wiley-Interscience, New York.

[8] Saucedo, L., Yu, R.C., and Ruiz, G. 2012. Fully-developed FPZ length in quasi-brittle materials. *International Journal of Fracture* **178**:97–112.

[9] Tvergaard, V., and Hutchinson, J.W. 1992. The relation between crack growth resistance and fracture process parameters in elastic-plastic solids. *Journal of the Mechanics and Physics of Solids* **40**(6):1377–1397.

[10] Xia, S., Takezono, S., and Tao, K. 1994. A nonlocal damage approach to analysis of the fracture process zone. *Engineering Fracture Mechanics* **48**(1):41–51.

[11] fib Model Code 2010. 2010. *Model Code for Concrete Structures 2010*. Fédération Internationale du Béton, Lausanne.

[12] Ruiz Carmona, J., and Ruiz López, G. 2017. Modelo analítico para el análisis de la flexión y la fisuración en secciones de hormigón armado como alternativa al diagrama de pivotes. *Hormigón y Acero* **68**(282):147–154.

[13] Eurocode 2. 2022. *Design of Concrete Structures*. European Committee for Standardization, Brussels.

[14] Ruiz, G., De La Rosa, Á., Wolf, S., and Poveda, E. 2018. Model for the compressive stress–strain relationship of steel fiber-reinforced concrete for non-linear structural analysis. *Hormigón y Acero* **69**:75–80.

[15] Ruiz, G., De La Rosa, Á., Poveda, E., Zanon, R., Schäfer, M., and Wolf, S. 2023. Compressive behavior of steel-fiber reinforced concrete in Annex L of the new Eurocode 2. *Hormigón y Acero* **74**(299-300):187–198.

[16] Ruiz, G., De La Rosa, Á., and Poveda, E. 2019. Relationship between residual flexural strength and compression strength in steel-fiber reinforced concrete within the new Eurocode 2 regulatory framework. *Theoretical and Applied Fracture Mechanics* **103**:102310.